Journal of
Synchrotron Radiation

ISSN 0909-0495

Received 8 August 2006
Accepted 19 March 2007

The Beamline X28C of the Center for Synchrotron Biosciences: a National Resource for Biomolecular Structure and Dynamics Experiments Using Synchrotron Footprinting

Sayan Gupta,[a,b] Michael Sullivan,[a,b] John Toomey,[a,b] Janna Kiselar[a,b] and Mark R. Chance[a,b]*

[a]Center for Proteomics and Mass Spectrometry, Case Western Reserve University, Cleveland, OH, USA, and [b]Center for Synchrotron Biosciences, National Synchrotron Light Source, Brookhaven National Laboratory, Upton, NY, USA. E-mail: mark.chance@case.edu

Structural mapping of proteins and nucleic acids with high resolution in solution is of critical importance for understanding their biological function. A wide range of footprinting technologies have been developed over the last ten years to address this need. Beamline X28C, a white-beam X-ray source at the National Synchrotron Light Source of Brookhaven National Laboratory, functions as a platform for synchrotron footprinting research and further technology development in this growing field. An expanding set of user groups utilize this national resource funded by the National Institute of Biomedical Imaging and Bioengineering of the National Institutes of Health. The facility is operated by the Center for Synchrotron Biosciences and the Center for Proteomics of Case Western Reserve University. The facility includes instrumentation suitable for conducting both steady-state and millisecond time-resolved footprinting experiments based on the production of hydroxyl radicals by X-rays. Footprinting studies of nucleic acids are routinely conducted with X-ray exposures of tens of milliseconds, which include studies of nucleic acid folding and their interactions with proteins. This technology can also be used to study protein structure and dynamics in solution as well as protein–protein interactions in large macromolecular complexes. This article provides an overview of the X28C beamline technology and defines protocols for its adoption at other synchrotron facilities. Lastly, several examples of published results provide illustrations of the kinds of experiments likely to be successful using these approaches.

Keywords: beamline; synchrotron footprinting; protein; nucleic acids; X-ray dose; hydroxyl radical; mass spectrometry.

1. Introduction

For several years synchrotron footprinting (SF) technology has been used to map the solvent accessibility of reactive probe sites in proteins and nucleic acids as a function of binding interactions, conformational changes and folding processes (Brenowitz *et al.*, 2002; Guan *et al.*, 2003, 2004; Guan & Chance, 2004, 2005; Maleknia *et al.*, 2001; Takamoto & Chance, 2004). SF combines a number of state-of-the-art techniques including the use of synchrotron radiation light sources (Gupta *et al.*, 2005; Maleknia *et al.*, 2001; Ralston *et al.*, 2000; Sclavi, Woodson *et al.*, 1998), the chemistry of radiolysis and interactions of the hydroxyl radical with nucleic acids and proteins in aqueous solution (Maleknia *et al.*, 1999; Sclavi *et al.*, 1997; Takamoto & Chance, 2004; Xu & Chance, 2004, 2005*a*,*b*; Xu *et al.*, 2003, 2005), mixing technologies to initiate rapid reactions (Johnson, 1986, 1995; Ralston *et al.*, 2000), and analytical tools for the detection of radiolysis products of nucleic acids and proteins (Guan & Chance, 2004; Kiselar *et al.*, 2002; Sclavi *et al.*, 1997; Sclavi, Woodson *et al.*, 1998; Takamoto & Chance, 2004; Takamoto, Chance & Brenowitz, 2004). These technologies have been implemented in the context of the X28C beamline facility at the National Synchrotron Light Source (NSLS) at Brookhaven National Laboratories. Recently, advancements in the beamline instrumentation, development of protocols for automated peak fitting to quantitate backbone cleavage in nucleic acids, and analytical advancements in examining radiolysis products in proteins by mass spectrometry have improved footprinting assays. This has allowed the examination of a wide range of

macromolecular interactions with femtomoles to picomoles of material under physiological solution conditions.

The facilities of the X28C beamline are available to international researchers, and the beamline activities are supported by the National Institute for Biomedical Imaging and Bioengineering. This review describes beamline X28C with examples of its impact in the field of structural biology.

2. Beamline instrumentation, operation and experimental methods

SF was developed at beamline X9A at NSLS and first applied to the study of RNA folding (Ralston *et al.*, 2000; Sclavi, Woodson *et al.*, 1998). A similar bending-magnet beamline, X28C, is currently dedicated to synchrotron footprinting research and its further development (Gupta *et al.*, 2005). The X28C beamline configuration is schematically outlined in Fig. 1. The beamline receives radiation from the NSLS X-ray storage ring, which circulates relativistic electrons with energies of 2.8 GeV at a maximum operating beam current of 300 mA. The water-cooled aperture situated 2.44 m downstream of the source defines the divergent beam in the beam-pipe that is aligned with the experimental set-ups inside the X28C hutch. The first upstream Be window situated at 8.86 m from the source separates out the ultra-high-vacuum (UHV) segment from the high-vacuum (HV) segment of the beam-pipe. A second Be window, situated at 14.66 m from the sources, separates out the HV segment from the beam-pipe in He atmosphere. The downstream end of this segment is capped by a third Be window, which is situated 14.90 m away from the source. The copper and lead aperture is bolted at the third Be window, which reduces the horizontal size of the beam to 20 mm and scattered radiation inside the hutch. The total thickness of the three Be windows is 750 µm (250 µm each), which limits the white beam inside the X28C hutch to an energy range of 5–20 keV. The beam travels an additional distance of 500 mm through a stainless-steel 'flight tube' capped with Kapton films (DuPoint Kapton, DuPoint). The flight tube is purged with He to maintain minimum contact of the beam with oxygen and reduce ozone generation. In addition, the beam-containment system minimizes scattered radiation in the hutch to reduce stray radiation on the samples. The beam finally falls on the experimental set-ups mounted on a precision motorized table. The horizontal size of the beam is large and the beam intensity is uniform up to several centimeters in width due to the large solid angle available in the unfocused bending-magnet configuration, However, the vertical emittance of the NSLS storage ring produces an unfocused beam of millimeter dimensions with a Gaussian profile and an intense 'hot spot' of <1 mm in height. A focusing mirror has been recently installed, which is located immediately downstream of the vacuum isolation Be window (Fig. 1). The mirror is single-crystal silicon coated with palladium with a cylindrical cut bendable to a toroidial form by motorized mirror benders. Control of the horizontal and vertical size of the beam on the sample can be achieved by changing the mirror angle and bender values. The mirror provides increases in the flux density of the X-ray beam on the sample, which is often useful in the study of large macromolecular complexes and fast (few millisecond) kinetic processes. A detailed report about the mirror and its usefulness in synchrotron footprinting studies will be published separately.

Fig. 2(*a*) schematically represents the experimental set-up inside the X28C hutch. A fixed 'stand' set-up consisting of an electronic shutter (Uniblitz, Model No. XPS6S2P1, Vincent Associates, Rochester, NY, USA) (Ralston *et al.*, 2000) and sample holder, or a KinTek quench flow (KinTek RQF3 Chemical Quench Flow, KinTek Corporation, Austin, TX, USA) (Johnson, 1986, 1995; Ralston *et al.*, 2000; Sclavi, Woodson *et al.*, 1998), are used to carry out controlled sample exposures. The X-ray irradiation of aqueous samples produces hydroxyl radicals by the radiolysis of water (Sclavi, Woodson *et al.*, 1998). It has been shown for beamline X9A that synchrotron X-ray beam characteristics provide a hydroxyl radical dose in a quasi-continuous manner (Sclavi, Woodson *et al.*, 1998). X-ray irradiation from a similar X-28C bending-magnet beamline maintains a steady-state concentration of

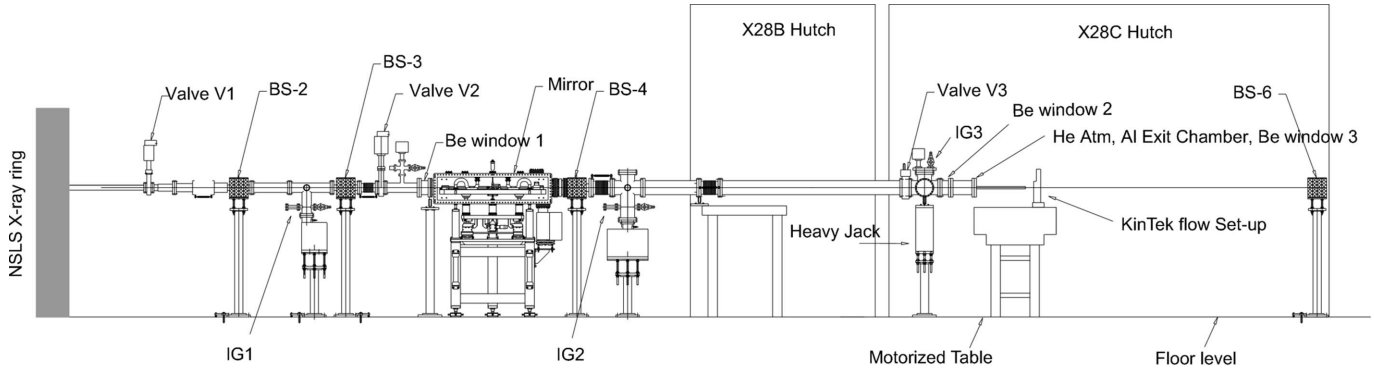

Figure 1
Schematic representation of the beamline X28C layout. The position of ion gauges (IG), bremsstrahlung shields (BS), valves, beryllium (Be) windows and the KinTek apparatus on the precision motorized table inside the X28C hutch are indicated. A cross-sectional view of the focusing mirror which resides between Be window 1 and BS-4 is indicated. The solid line indicates the pathway of the unfocused beam.

hydroxyl radicals during the exposure time of the order of milliseconds and delivers doses that are sufficient to provide suitable oxidative changes in biological macromolecules (Sclavi, Woodson *et al.*, 1998). The sample concentrations are extremely low compared with the concentration of bulk phase water; therefore direct interactions between X-rays and the nucleic acids or protein remain negligible. Thus the effects of the radiation are entirely indirect and mediated by the oxidation products of water. The issues of chemistry of radiolysis, X-ray dose and energy deposition have been previously reviewed (Guan & Chance, 2004; Ralston *et al.*, 2000; Sclavi, Woodson *et al.*, 1998).

2.1. Conducting a steady-state experiment with the stand set-up

The stand set-up, consisting of an electronic shutter and aluminium sample holder, is mounted on the precision motorized table for carrying out equilibrium and manual mixing kinetic experiments (Fig. 2*a*). In a typical steady-state experiment, samples are distributed in the bottom of 200 µl microcentrifuge tubes in aliquots of 5 µl and exposed one at a time by placing the tubes on the sample holder. The electronic exposure shutter controls the exposure time on the millisecond time scale. It is equipped with a 1 mm platinum/iridium alloy plate capable of blocking X-rays up to energies of 30 keV. Fluorophor assays of X-ray dose, discussed below, show that the shutter blocks almost 99% of the X-ray beam from falling on the sample. This shutter operates reliably for exposure times as short as 7 ms. During the experimental run the temperature of the aluminium sample holder is controlled by a temperature-regulated circulating water bath within the range 274–315 K. The temperature of the sample holder can also be adjusted to 243 K with the help of a cryo-cooler unit for experiments with frozen samples. For protein footprinting experiments, methionine amide is added to a final concentration of 10 m*M* to prevent peroxide-induced secondary oxidation reactions (Xu *et al.*, 2005). Generally no quencher is added for nucleic acids footprinting experiments. Exposed samples are frozen in dry ice and stored at 193 K before further processing.

2.2. Conducting time-dependent footprinting studies with a KinTek quench flow set-up

To conduct millisecond kinetic experiments, the stand set-up is removed from the path of the beam and a modified KinTek quench-flow apparatus (Sclavi, Woodson *et al.*, 1998)

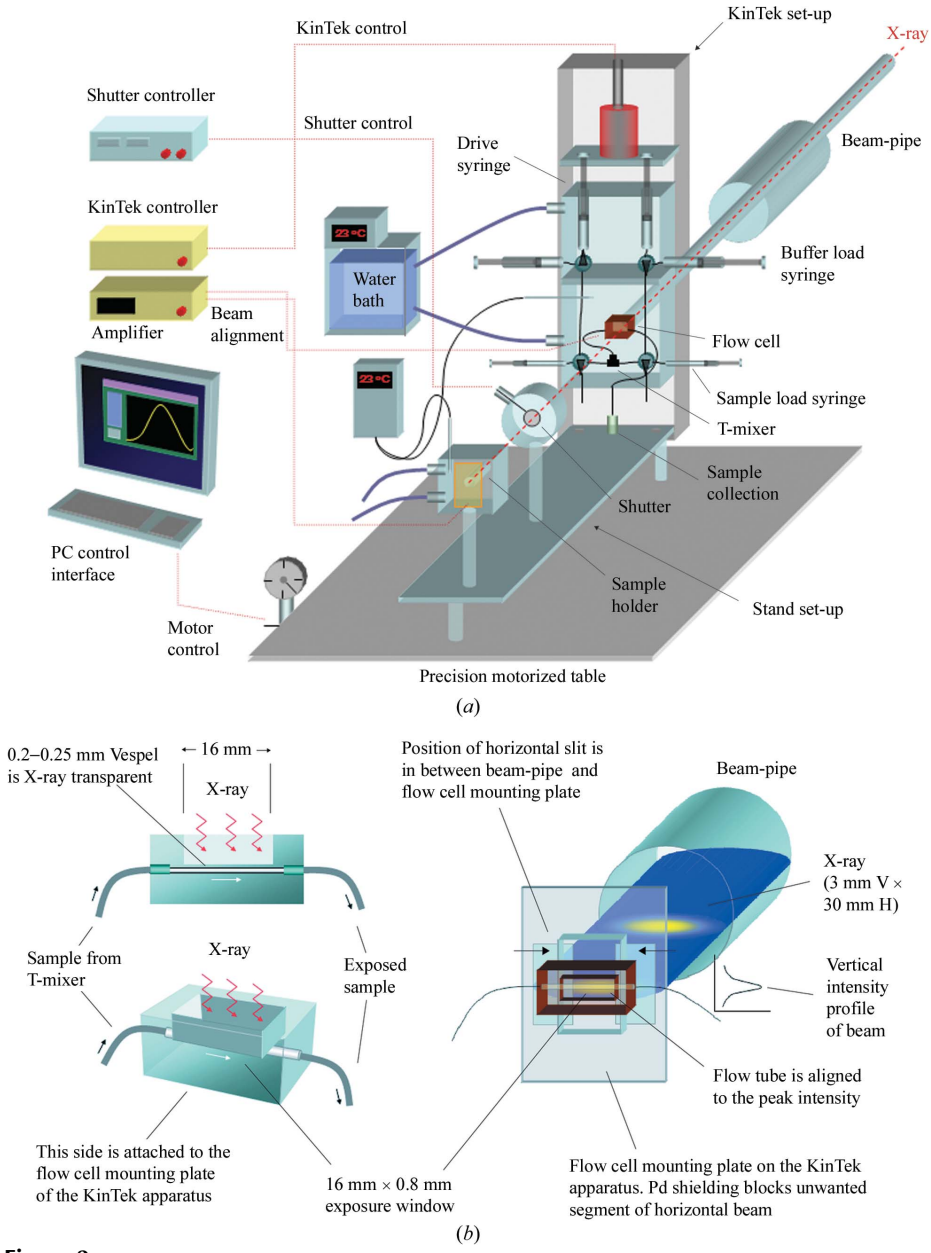

Figure 2
Schematic representations of the experimental set-up in beamline X28C. (*a*) The stand set-up and the KinTek quench-flow apparatus are mounted separately on the precision motorized table along the beam path inside the hutch. The exposure chambers for both set-ups are aligned to maximize the intensity of the beam. The PC interface for the beam alignment, KinTek controller and the shutter controller are situated outside the X28C hutch. (*b*) The design of the flow cell is shown on the left-hand side. The sample residing inside the 0.8 mm-diameter flow-path is exposed through a 0.2–0.25 mm-thick and 16 mm-wide Vespel window. The right-hand panel schematically represents the position of the flow cell attached to the mounting plate (the entire apparatus is not shown) on the KinTek apparatus, the position of the horizontal slit assembly, the X-ray beam and beam-pipe after a vertical beam alignment. Reproduced with permission from Gupta *et al.* (2005).

is installed on the precision motorized table (Fig. 2*a*). The samples are loaded in the sample loop using a load syringe; the sample volume can be varied in the range 5–50 µl. The two solutions are rapidly mixed through a T-mixer and then, after the given delay time, the reaction mixture is passed through the flow cell for sample exposure. The rate of the sample flow at each step, *i.e.* loading, mixing, delay, exposure and collection, are controlled by the KinTek stepper motor controller software program *PACCOM* (version 3.20), from Pacific Scientific Digital Motion Control Products. In order to prevent scattered radiation from falling on the sample during exposure, lead shielding is placed on the rear plate of the flow apparatus surrounding the flow cell and the sample load syringe. The temperature surrounding the flow tubes and the flow cell is controlled by a circulating water bath, which also provides additional protection from unwanted scattered radiation during the experimental run.

The flow cell, shown in Fig. 2(*b*), is made from a block of Vespel (DuPoint Vespel, DuPoint), a material that can withstand prolonged exposure to the white synchrotron beam. It has a machine-drilled cylindrical sample flow-path passing through the center of the block with a radius of 0.8 mm. A 16 mm × 5 mm block is cut out from the 'front' of the flow cell to create a rectangular void in front of the drilled flow path. The void faces towards the X-ray beampipe. The distance between the void and the flow path ranges between 0.2 and 0.25 mm. The thickness of the Vespel material acts as a transparent window for the white X-ray beam. This flow cell is specifically designed to expose the samples most efficiently with the current beamline configuration, which provides a small vertical beam and a wide horizontal beam. The exposure time is controlled by combination of the exposure sample volume, volume of solution expelled by a single revolution and varying speeds of the KinTek stepper motor. The exposure time is determined from the following equation for the existing set-up available in the operation manual for the RQF3 Chemical Quench Flow,

$$\text{exposure time [ms]} = \frac{\text{exposure sample volume [µl]} \times 60 \times 10^3}{847\ \text{[µl]} \times \text{motor speed [r.p.m.]}}.$$

The existing flow cell has an exposure sample volume of 8.0 µl [16 mm (horizontal length) × 0.16 mm^2 (0.4 mm radius) × 3.14]. A very short exposure time of 2.3 ms can be accomplished with the maximum motor speed of 250 r.p.m. in the existing set-up of KinTek. However, it is possible to further reduce the exposure time by decreasing the exposed sample area. A horizontal slit mounted in front of the flow cell is used to reduce the horizontal size of the beam or the exposed area on the sample and consequently the exposure time frame. In the presence of unfocused beam, we need a minimum of 10–30 ms exposure to obtain considerable sample modification and/or cleavage. Recently the focused beam has been used to accomplish single digit exposure time in milliseconds. The exposed samples are collected in microcentrifuge tubes. Samples are frozen in dry ice and stored at 193 K.

2.2.1. Exposure of a large volume of samples and cells for steady-state footprinting. The KinTek quench-flow mixer can be modified so that a single syringe pushes the sample directly from a sample loop into the flow cell. The size of the sample loop in this modified set-up can vary from 50 µl to 1 ml. If the sample volume is larger than 1 ml then the entire loop can be by-passed and the drive syringes can be used for sample loading up to a volume of 5 ml. These modifications allow exposure of the entire volume of the sample in a single step. Depending on the sample volume and exposure time, the flow rate is adjusted in the usual way by changing the steps and revolution speed of the KinTek stepper motor using the KinTek controller software program. This continuous-flow set-up allows exposure of large volume samples on a time scale from 0 to 300 ms. This is convenient when a low-concentration sample is being examined. The exposed samples are collected in the usual way and frozen in dry ice and stored at 193 K. This method is also used to expose cell preparations for the development of cellular footprinting approaches.

2.3. Beam alignment

The position of the sample is aligned to overlap with the most intense spot of the beam for uniform and efficient sample exposure. The beam alignment is carried out by a vertical scan of X-ray intensity using a precision motorized table and simultaneously detecting the X-ray signal from the incident X-ray beam at the position of the sample exposure chamber. A 12 V servo motor driven by a MicroMo servo controller is used and interfaced with a Windows-based computer running National Instrument's *LabView* software to operate the scanning of the motorized table. In the stand set-up a photodiode detects the beam through a 50 µm vertical slit mechanically mounted just behind the sample exposure chamber. The measured signal is converted into an output file by the *LabView* software for further analysis. The most intense beam position is determined from the mid-point of the Gaussian vertical-beam profile. The precision motorized table is moved to the most intense position by the same motor control software to align the exposure chamber to the position of the peak intensity. In the KinTek set-up an external photodiode assembly is placed in front of the flow cell that allows alignment of the peak intensity exactly along the 16 mm flow path in a similar way. In both cases the beam is attenuated by multiple layers of 1.2 mm-thick aluminium plates to prevent direct irradiation of the photodiode detector by intense X-rays. The signal intensity of the attenuated beam is adjusted by controlling the gain in a UDT amplifier (UDT Instrument MD 301-DIV Position Monitor Unit) which is interfaced with the Windows-based computer running the *LabView* software. The size of the focus beam varies in both the horizontal and vertical direction depending on the mirror angle and bender values. Developments of new alignment devices useful for the focused beam are in progress.

2.4. Sample preparation, shipment and storage

SF experiments are generally carried out with sample concentrations ranging from picomolar to micromolar in 10–30 m*M* in phosphate or cacodylate buffer. At appropriate pH

values these buffers are optimal to reduce scavenging (see §3). With the availability of the brighter beam other biological buffers might be useful. Samples are most often prepared at the home institution and then shipped to the beamline in ice or in dry ice. Buffer exchange or any dilutions for non-radioactive samples are carried out at a designated work-bench outside the X28C hutch. All radio-labeled nucleic acid samples are shipped in small aliquots strictly following the radiological work permit issued by the Brookhaven National Laboratories. All radiological work is carried out under compliance of ^{32}P handling protocols specific for the X28C beamline. Once exposed, the non-radioactive samples are stored at 193 K for further analysis or shipped back to the respective user institutions. Exposed radio-labeled samples are stored in a special lead box in a 253 K freezer inside the X28C hutch. The freezer is covered by a 4.03 mm-thick lead sheath to prevent unwanted exposure due to scattered radiation in the hutch. All radio-labeled samples are shipped back to the user institution by strictly following the X28C ^{32}P protocol.

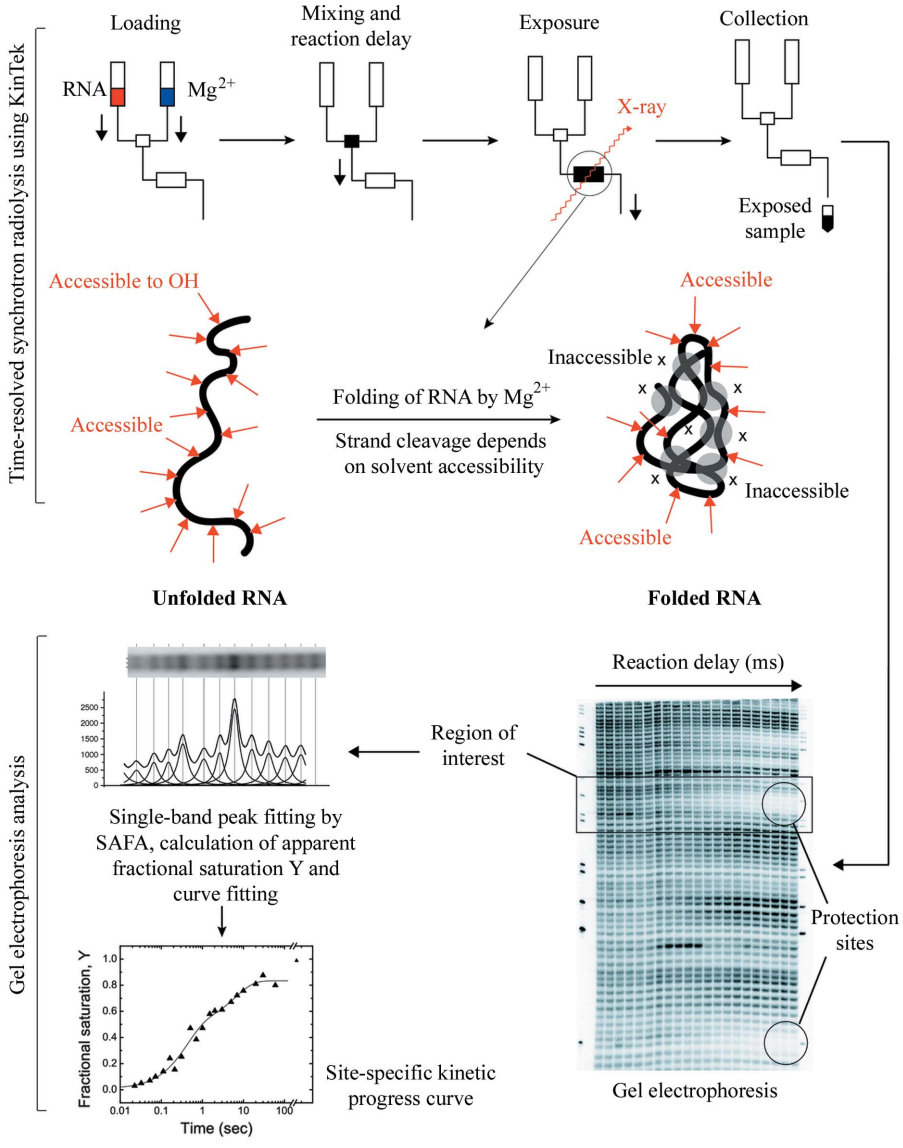

Figure 3
Schematic representation of nucleic acid footprinting using synchrotron radiolysis and quantitative PAGE. The upper panel shows the method for conducting a kinetic experiment using the KinTek apparatus. Unfolded RNA and Mg^{2+} are mixed through a T-mixer and allowed to react for various time intervals or delay times. After each reaction delay the samples are exposed to X-rays for 10 or 15 ms in the flow cell. When RNA folds, it can form discrete tertiary regions of contact which become inaccessible to the solvent; hence those regions show less strand cleavages. When PAGE is run with the exposed sample in the presence of appropriate controls, as indicated in the lower panel, the reduced strand cleavages appear as reduced band intensities. These regions of reduced intensity are termed 'protections'. The 'single-band analysis' technique is used for the quantification of the bands. By this procedure, total intensities of the bands are converted to 'Y', fractional saturation. Y is proportional to the amount of cleavage in the nucleotide backbone. Any time-resolved experiment generates a set of Y values with respect to various reaction times. A non-linear regression curve fitting of Y against time reveals the kinetic progress curve of the folding process with a single nucleotide.

2.5. Data acquisition and analyses

Nucleic acids in solution undergo strand cleavages upon exposure to X-rays; the extent of the strand cleavage depends on the solvent accessibility of the nucleic acid backbone (Brenowitz *et al.*, 2002; Maleknia *et al.*, 2001; Takamoto & Chance, 2004). The binding of ligands or folding of domains can change the solvent accessibility at specific sites attenuating the extent of strand cleavage. When the exposed samples are analyzed using polyacrylamide gel electrophoresis (PAGE), the extents of stand cleavage are revealed as a clear footprint in the gel pattern when compared with the control gel bands (Takamoto & Chance, 2004). Quantitative analysis of the band intensities from either ^{32}P or fluorophor-labeled nucleic acids fragments are then carried out using densitometric software and 'box analysis' or 'single-band analysis' where the band intensities of interest are digitized (Takamoto & Chance, 2004; Takamoto, Chance & Brenowitz, 2004). An overview of the steps in a nucleic acid footprinting experiment (in this case the time-resolved folding of an RNA molecule is illustrated) is schematically depicted in Fig. 3. For kinetic studies the normalized extent of strand cleavage is monitored as a function of time after the administration of a suitable reagent to stimulate the folding, unfolding or any ligand binding processes (Sclavi, Sullivan *et al.*, 1998; Takamoto & Chance, 2004). Equilibrium isotherms are generated by titration with the reagent and analyzing the level of protection conferred as a function of the

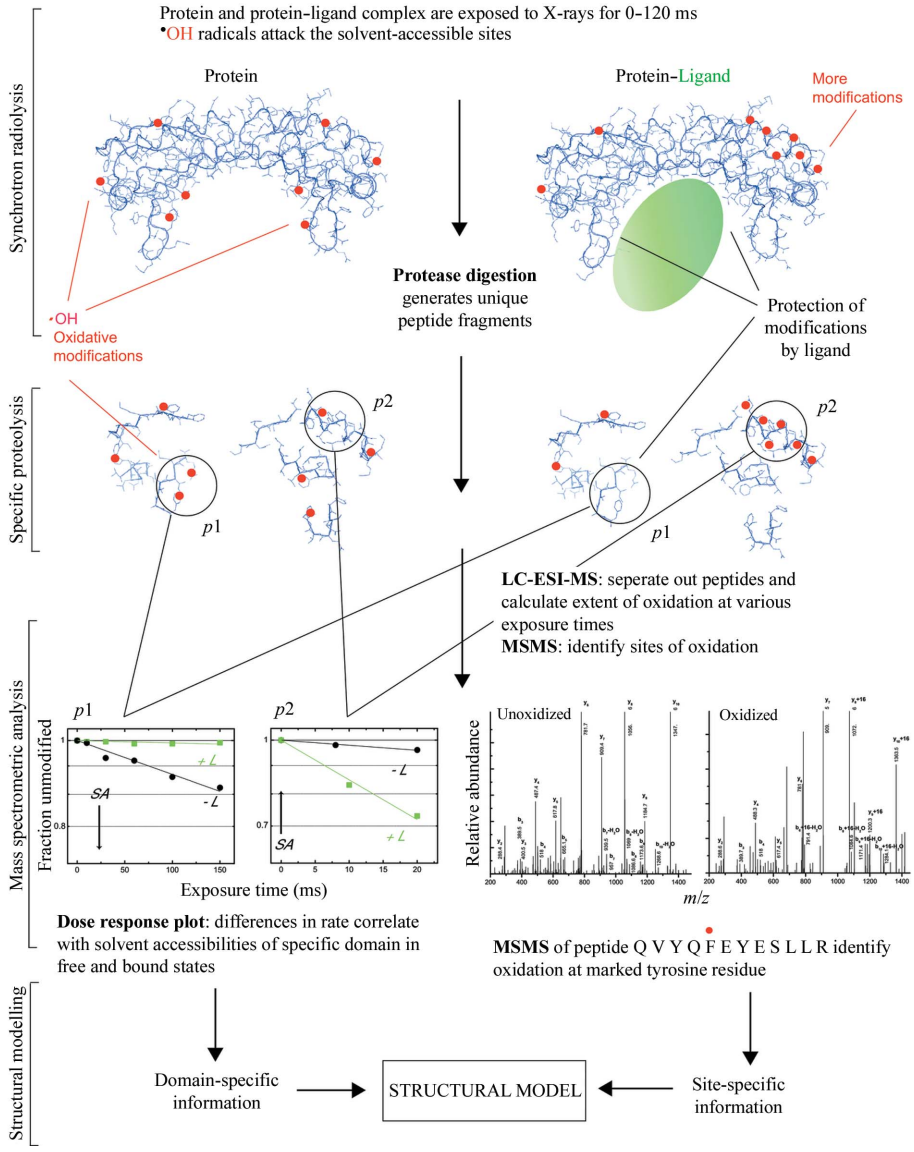

Figure 4
Schematic representation of protein footprinting using synchrotron radiolysis and mass spectrometry. The examples emphasize the protection formed in the interface of a protein–ligand complex as well as allosteric conformation changes that can result in increases in reactivity upon ligand binding; however, the comparison could be for any two (or multiple) functional states of the protein of interest. Two sets of samples, one free protein and the other a protein–ligand complex, are exposed to X-rays for different time intervals. The exposed samples are digested with specific digestion enzymes. The digested fragments are analyzed by ESI-MS to quantitate the extent of modification products and determine the fraction 'unmodified' for a specific exposure time. A plot of fraction unmodified *versus* exposure time, known as the dose response plot, fit to a first-order function providing the rate of modification for the specific peptide. Comparisons of the dose response of the same peptide under different conditions provide structural information about ligand binding. MS/MS is used to determine the specific modification site within the peptide and provide side-chain-specific structural resolution. Synchrotron protein footprinting data are often used as one of the constraints in model building for complexes.

reagent concentration (Dhavan *et al.*, 2002; Takamoto & Chance, 2004). In this case a fixed exposure time is used to generate strand cleavage optimized for the experimental systems under study.

The reactions between protein molecules and hydroxyl radicals result primarily in chemical modification of the amino acid side-chains (Guan & Chance, 2004; Gupta *et al.*, 2005; Kiselar *et al.*, 2002; Maleknia *et al.*, 1999, 2001). Unlike the case for nucleic acids, the reaction is not solely dependent on the solvent accessibility of the reactive site as the intrinsic reactivity of the amino acid side-chains varies considerably (Kiselar *et al.*, 2002). Electro-spray-ionization mass spectrometry (ESI-MS), tandem MS and matrix-assisted-laser-desorption-ionization mass spectrometry (MALDI-MS) are used to identify the sites and determine the extents of the hydroxyl-radical-induced side-chain modification products generated in peptides and proteins (Kiselar *et al.*, 2002). These approaches have been recently reviewed and are not extensively discussed here (Takamoto & Chance, 2006; Xu & Chance, 2004, 2005*b*; Xu *et al.*, 2003, 2005). Briefly, 14 of the 20 side-chains show detectable modification products and are likely to be useful for the quantitation of the extent of modification in footprinting experiments. The overall footprinting experiment is summarized in Fig. 4. Similar to that of its nucleic acid counterparts, protein footprinting experiments can be performed in a time-resolved fashion using the rapid flow mixer in the X28C beamline.

3. Dose optimization for footprinting assay

The extent of exposure or the radiolytic dose received by a sample in SF experiments is directly proportional to the amount of hydroxyl radicals produced upon X-ray irradiation. In SF experiments the dose is controlled such that, for nucleic acids cleavage, each molecule that is cleaved, is cleaved only once on average (Sclavi, Woodson *et al.*, 1998). For protein footprinting experiments the dose is optimized such that the loss of unmodified peptide products follows an apparent first-order reaction (Maleknia *et al.*, 2001; Takamoto & Chance, 2006). As for nucleic acids, protein samples have a diverse distribution of solvent-accessible and reactive sites. Hence, under the same dose level, the modification levels will vary considerably within different protein samples. Several other factors, such as synchrotron beam current, buffer composition and concentration, presence of metal ion chelators (*e.g.* EDTA, EGTA *etc.*), cofactors (*e.g.* ATP, ADP *etc.*), reducing agents (*e.g.* dithiothreitol, β-marcaptoethanol *etc.*) or stabilizing agents (*e.g.* glycerol,

polyethylene glycol, sucrose *etc.*), can also affect radiolytic dose.

A novel approach has been adapted to predict the radiolytic dose that is required to generate a sufficient amount of radiolytic modifications under any experimental conditions. This is carried out by monitoring the radiolytic degradation of Alexa fluorophor by the X-ray beam under defined conditions of protein and/or buffer. Alexa fluorescence is abolished by X-ray exposure with apparent first-order kinetics. Fig. 5(*a*) shows a typical dose response plot of Alexa 488 radiolysis with the stand set-up; the observed rate constant is a relative measure of the radiolytic dose. In this example the fluorescence signal is depleted by X-ray exposure at a rate of 40 s^{-1}. Although the unique characteristics of biological samples cannot be predicted, those of buffer components can be established and thus anticipated. In the following section we describe several examples of the use of Alexa radiolysis as a sensor to detect the radiolytic dose at the beamline. This approach is entirely general and can also be used to compare the flux and useful energy content of a wide range of X-ray beamlines, as well as other possible radiolysis sources and radical generators such as Fenton or photolysis of peroxides (Takamoto & Chance, 2006).

The amount of hydroxyl radicals generated in biological samples is directly proportional to the beam flux, which in turn is proportional to the electron beam current of the synchrotron ring. The beam current at NSLS decays exponentially from the maximum refill current of ~300 mA as a function of elapsed time after each refill of the electron storage ring. These refills typically occur at 12 h intervals to replenish the beam current value. Hence, an experiment carried out at ~290 mA current will receive a higher dose compared with that at 200 mA, and the radiolytic rate constants obtained from two such experiments have to be calibrated to eliminate the change associated with differences in X-ray dose. Instead of making a calibration curve for every biological system

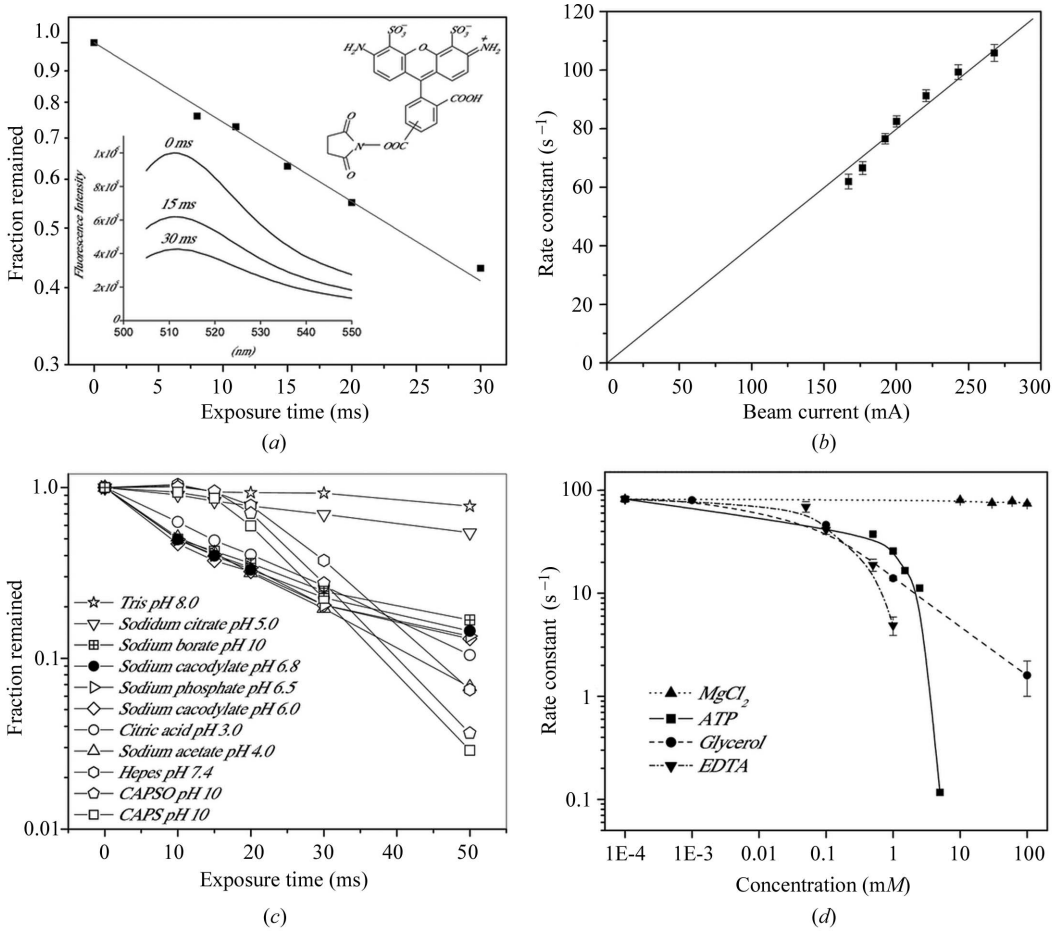

Figure 5
Alexa radiolysis and determination of X-ray dose. (*a*) Dose response plot of 1.0 μ*M* Alexa 488 in 10 m*M* sodium cacodylate pH 7.0 buffer containing 0.1 m*M* EDTA irradiated with synchrotron X-rays at 190–220 mA beam current. After exposure the Alexa is diluted (1:500) prior to fluorescence analysis. A Turner Biosystems TBS-380 fluorometer is used to determine the emission intensity at 516 nm with an excitation wavelength of 496 nm. The solid line represents the fitting of data to a first-order reaction kinetics. The insets in the top right and the bottom left corners show the dye structure and the decrease in fluorescent emission caused by irradiation at different times, respectively. (*b*) Rate constant of 1.0 μ*M* Alexa 488 in 10 m*M* sodium cacodylate pH 7.0 buffer without EDTA as a function of the beam current. The solid line represents the linear fit with a slope of 0.41 ± 0.03 s^{-1} mA^{-1}. (*c*) Dose response plots of 1.0 μ*M* Alexa 488 in 10 m*M* of different buffers. (*d*) Rate constant of radiolytic degradation of 1.0 μ*M* Alexa 488 in 10 m*M* sodium cacodylate pH 7.0 buffer with addition of $MgCl_2$, ATP, glycerol and EDTA at different concentrations. The connections between the points are represented by respective spline-lines.

under study, which is a rather lengthy process, Alexa radiolysis is used to generate a general calibration curve for experimental conditions of various kinds. The decay rates of Alexa at various beam current values are shown in Fig. 5(*b*). Two features of this curve are encouraging. First, the rate of decay of the Alexa fluorophor is linear in beam current, indicating that the method used to examine dose behaves as expected. Second, the curve intersects the axis at zero oxidation rate implying there is no significant background or secondary oxidation process that is sufficiently reactive to modify the fluorophor.

Buffer composition also affects radiolytic dose in aqueous samples. Fig. 5(*c*) shows a dose response for Alexa 488 in various buffers at 10 m*M* concentration and at pH values ranging from 3 to 10. The radiolysis of Alexa 488 in sodium cacodylate or phosphate buffers follows an apparent first-order kinetics and has rates close to those of Alexa in water. These buffers are thus reasonable for footprinting experiments because of their minimum quenching of the hydroxyl radical. The data also indicate that citric acid, sodium acetate and sodium borate buffers are suitable for footprinting experiments at pH values of 3.0, 4.0 and 10.0, respectively.

HEPES, CAPSO, CAPS (Fig. 5*c*) and MOPS (data not shown) buffers show dose response curves that significantly deviate from apparent first-order kinetics. They show similar trends with a lag phase lasting until ∼30 ms of exposure, followed by a sudden burst of considerable degradation. A plausible explanation is that in the initial phase the buffer molecules interact with the hydroxyl radicals faster than the radicals react with the fluorophor. Once a sufficient quantity of buffer molecules react, and are somewhat depleted, the Alexa oxidation increases leading to the second phase. Sodium citrate and Tris-HCl buffers also significantly quench the degradation of the fluorophor. These buffers are not as suitable for radiolysis experiments because of the quenching of hydroxyl radicals, and the variability of rate. In addition, the possible destruction of buffer molecules may lower the buffering capacity of the solution.

Different additives such as glycerol, ATP, EDTA or divalent salts such as $MgCl_2$ are frequently included in biological samples to promote sample stability or folding. Glycerol is generally used for many protein samples to promote stability during storage. Fig. 5(*d*) shows the effect of glycerol on the degradation rate of Alexa 488, indicating that even 1.0 m*M* of glycerol can diminish the rate of Alexa oxidation by a factor of five, implying that a five-fold increase in dose is required to achieve the same level of modification or cleavage compared with the case in the absence of glycerol. Thus, thorough removal of glycerol is an essential step prior to footprinting experiments unless flux density is enhanced by using the focusing mirror. Flurophor assay has established that a 100-fold increase in the flux density is attainable by the use of a focusing mirror (data not shown). In the samples where the presence of certain amounts of glycerol is necessary for the stabilization of macromolecular complexes, an Alexa radiolysis assay can help experimenters adjust the exposure time accordingly to overcome the quenching of the hydroxyl radical by glycerol. Fig. 5(*d*) also indicates the quenching effects of ATP and EDTA. Unlike these organic molecules, inorganic ions do not show any quenching of hydroxyl radicals.

4. Recent results

With the growing development of mass spectrometry tools for the study of proteins and the advances in the time-resolved apparatus developed at X28C, SF has become a promising approach for demonstrating structure–function relationships for biological macromolecules in solution. The following section provides results illustrating applications of SF technology that have been carried out using the X28C facility.

4.1. Conformational activation in gelsolin

Gelsolin, schematically represented in Fig. 6(*a*), is a Ca^{2+}-dependent actin regulatory protein composed of six homologous subdomains that severs actin filaments and caps the fast-growing barbed end of actin filaments inside the cell. Radiolytic protein footprinting provided details with respect to the structural changes that occur as a function of Ca^{2+}-dependent activation of gelsolin in solution (Kiselar *et al.*, 2003*a*,*b*). More that 80 discrete peptide segments, covering

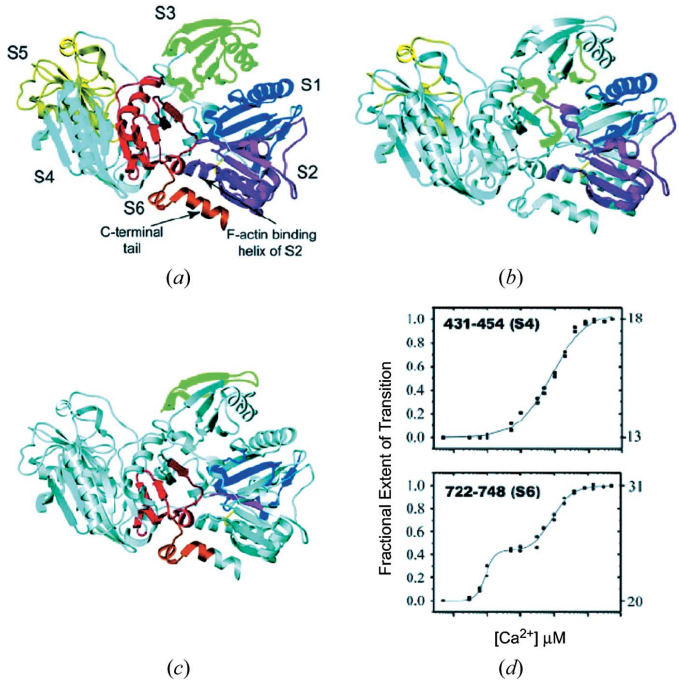

Figure 6
Synchrotron footprinting of the Ca^{2+}-dependent conformational activation of gelsolin. (*a*) Subunit structure of gelsoline. Individual colors correspond to specific subdomains. (*b*) Peptides that are oxidized but the extent of oxidation does not change as a function of Ca^{2+} concentration. The peptide locations are color coded according to the subdomain where they are found as per (*a*). (*c*) Peptides that were sensitive to Ca^{2+} concentration. The peptide locations are color coded according to the subdomain where they are found as per (*a*). (*d*) Representative Ca^{2+} titration isotherm for the peptide *p*431–454 and *p*722–748 in domains S6 and S4, respectively. Each symbol is generated from a single experiment showing the extent of oxidation after exposure of gelsolin to X-rays for 80 ms at a specific concentration of Ca^{2+}. Reproduced with permission from Kiselar *et al.* (2003*b*).

95% of the sequence of gelsolin, were examined by mass spectroscopy before and after radiolysis to probe their solvent accessibilities as a function of Ca^{2+} concentration in solution. Dose response data revealed 22 tryptic peptides that exhibit detectable oxidation and seven among them showed Ca^{2+} sensitivity to oxidation extent. Five peptides in subdomains S1, S2, S4 and S6 showed increases in oxidation extent and the remaining two in peptides subdomains S3 and S6 showed decreases in the extent of oxidation in the presence of 200 µ*M* Ca^{2+} compared with no added Ca^{2+}. Figs. 6(*b*) and 6(*c*) summarize the footprinting protection map providing information on the domain-specific Ca^{2+}-dependent conformational rearrangements within gelsolin. Five peptides that undergo increases in radiolytic oxidation show complex changes in the extent of oxidation as a function of Ca^{2+} concentration. The Ca^{2+} titration isotherms as represented in Fig. 6(*d*) showed a distinct intermediate that is significantly populated in the 1–10 µ*M* concentration range of Ca^{2+} based on data from peptides in the S1, S2 and S6 domains. In contrast, a peptide in domain S4 exhibited no intermediate state in its conformational transition. Tandem MS results were used to identify the specific side-chains that are sensitive to oxidation. The extent of oxidation of the numerous residues within gelsolin subdomains indicated that the structural reorganization associated with the Ca^{2+} binding is extensive and demonstrates a differential role for N- and C-terminal halves of the molecule.

4.2. RNA folding

SF was utilized to analyze the relationship of metal ion concentration and tertiary structure and folding of the *Tetrahymena* ribozyme. The high flux of the SF method is ideal for millisecond time-resolved studies. This has been successfully applied to follow the folding of RNAs as a function of divalent metal ion.

The kinetics of folding of the *Tetrahymena* ribozyme [summarized in Fig. 7(*a*)] was first observed to a time resolution of milliseconds using SF. These studies showed that the native tertiary contacts of the P5c subdomain form first ($\sim$2 s^{-1}), followed by those of the P4–P6 domain ($\sim$1 s^{-1}), the peripheral helices (0.2–0.4 s^{-1}) and lastly the catalytic core ($\sim$0.03 s^{-1}). These observations led to the novel conclusion that the organization of the catalytic core occurs within the constraints of the structures formed by the peripheral helices and P4–P6 (Sclavi, Sullivan *et al.*, 1998). The P4–P6 domain was proposed to act as a folding scaffold for the *Tetrahymena* ribozyme; this was further illustrated by SF studies on the isolated P4–P6 domain (Silverman *et al.*, 2000). SF has shown that Mg^{2+}-dependent folding of the *Tetrahymena* ribozyme is

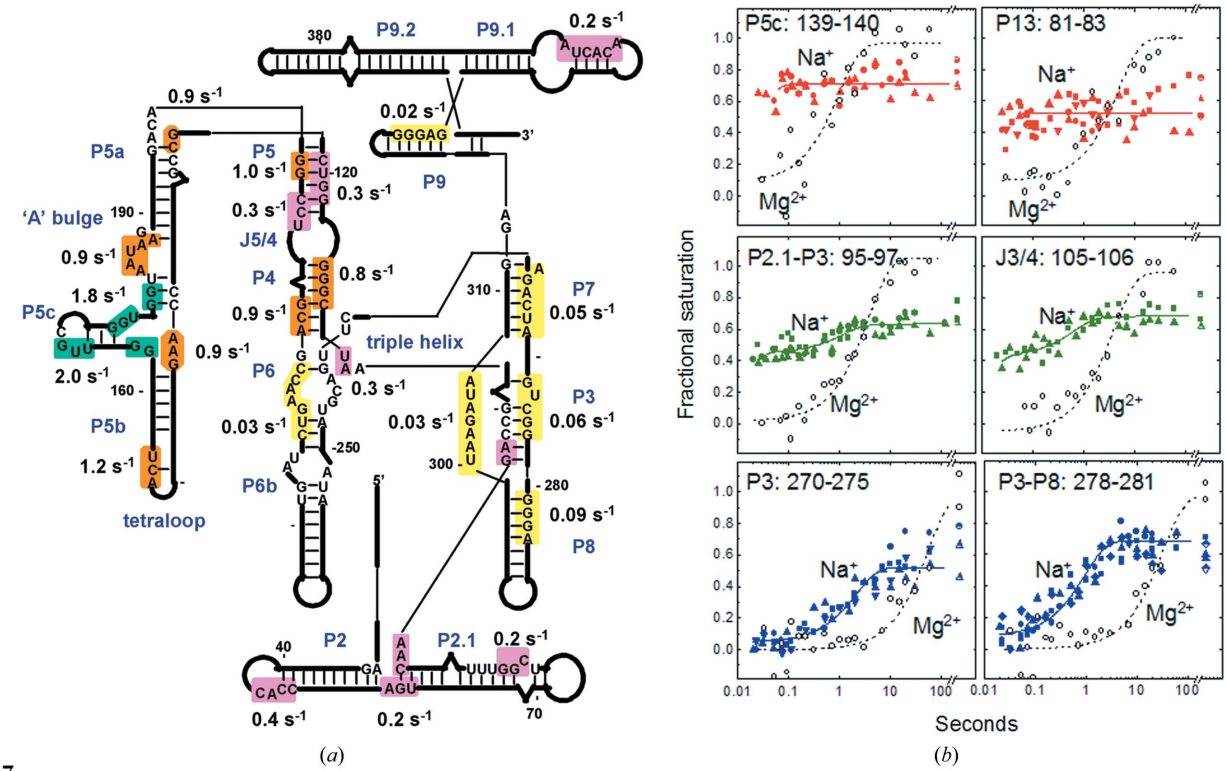

Figure 7
Synchrotron footprinting of *Tetrahymena* L-21 ribozyme with a synchrotron X-ray beam. (*a*) A summary of the Mg^{2+}-mediated folding rates obtained from the similar kinetic progress curves as shown in (*b*) mapped onto a secondary structure representation. Represented with permission from Sclavi, Sullivan *et al.* (1998). (*b*) Kinetic progress curves comparing the Na^+ (solid symbols) and Mg^{2+} (open symbols) mediated folding of *Tetrahymena* ribozyme. In both cases folding was initiated from cacodylate-EDTA buffer containing 0.008 *M* Na^+ to a final concentration of 1.5 *M* NaCl and 10 m*M* $MgCl_2$, respectively. The solid lines are fits to single or multiple exponential functions. Each symbol type represents an independent experiment. Each panel is labeled with the region of the *Tetrahymena* ribozyme whose hydroxyl radical reactivities were determined. Reproduced with permission from Shcherbakova *et al.* (2004).

greatly accelerated by increasing the concentration of monovalent cations (Shcherbakova *et al.*, 2004; Uchida *et al.*, 2003). Fig. 7(*b*) shows a representative set of kinetic progress curves for the individual tertiary contacts obtained by Na^+ or Mg^{2+} ions. Significant differences are clearly evident in the folding kinetics induced by monovalent *versus* divalent cations. Both monovalent and divalent metal ions can change the preferred folding pathways by selectively stabilizing particular structural motifs. Most recently, SF studies on the folding pathways of the 16s rRNA 5′ domain revealed that it can form all of the predicted tertiary interactions in the absence of proteins (Adilakshmi *et al.*, 2005). This supports the idea that the intrinsic folding of the rRNA can dictate the hierarchy of the ribosome assembly that guides the initial phase of RNA–protein interactions and establishes the structural platform for subsequent steps in the 30S ribosome assembly. The local changes in the solvent accessibility deduced from profiles of the hydroxyl radical reactivity can be integrated effectively with global reports of nucleic acid structure such as small-angle X-ray scattering (SAXS) and analytical ultracentrifugation studies to provide a complete picture of macromolecular interactions (Kwok *et al.*, 2006; Takamoto, Das *et al.*, 2004).

5. Conclusion and future directions

Approaches to study macromolecular structure and dynamics in solution using SF have been facilitated by the construction and operation of the beamline X28C. As described by the examples presented in this report, synchrotron X-rays with high flux density make SF a valuable tool for the biological sciences. Beamline X28C at the National Synchrotron Light Source is designed to provide user support to the scientific community and serves as a model for developing similar facilities in other synchrotron sources. The SF technique in the X28C facility continues to have unique capabilities, one of which is the prospect of examining macromolecular structure *in vivo*. Proof that such approaches are feasible was recently demonstrated by a user at X28C (Adilakshmi *et al.*, 2006); this provides an exciting new avenue for technology development for the resource. Recently, laboratory-based methods of carrying fast-hydroxyl radical footprinting for nucleic acids have been demonstrated; this development has been stimulated by the advent of the SF methods and will allow a wider range of laboratories to access these types of experiments (Shcherbakova *et al.*, 2006). The availability of the controlled X-ray dose in the X28C facility allows researchers to precisely measure the extent of oxidation in the amino acid side-chains *versus* exposure time, which is rather difficult to achieve by other laboratory-based methods. The synchrotron approach can uniquely examine structure for sulfur-containing amino acids compared with laboratory-based methods that use peroxide for oxidation. Recently it has been shown that it acts as a valuable probe in protein footprinting studies with large macromolecular assemblies (Kiselar *et al.*, 2007). Beamline X28C continues as a platform for the development of new applications and technologies for the determination of the structure of larger biomolecular assemblies. Currently, beamline developments are also in progress for the automation of sample handling techniques and accomplish faster time-resolved experiments using the focused beam. The future plans to improve the beamline facility include use of increased flux density obtained from the focusing mirror to overcome the effects of intrinsic and extrinsic scavengers present in biological samples, the study of large biomolecular complexes (>250 kDa), and the structure of membrane proteins both *in vitro* and *in situ*.

This research is supported in part by The Biomedical Technology Centers Program of the National Institute for Biomedical Imaging and Bioengineering (P41-EB-01979).

References

Adilakshmi, T., Lease, R. A. & Woodson, S. A. (2006). *Nucl. Acid Res.* **34**, e64.
Adilakshmi, T., Ramaswamy, P. & Woodson, S. A. (2005). *J. Mol. Biol.* **351**, 508–519.
Brenowitz, M., Chance, M. R., Dhavan, G. & Takamoto, K. (2002). *Curr. Opin. Struct. Biol.* **12**, 648–653.
Dhavan, G. M., Crothers, D. M., Chance, M. R. & Brenowitz, M. (2002). *J. Mol. Biol.* **315**, 1027–1037.
Guan, J. Q., Almo, S. C. & Chance, M. R. (2004). *Acc. Chem. Res.* **37**, 221–229.
Guan, J. Q., Almo, S. C., Reisler, E. & Chance, M. R. (2003). *Biochemistry*, **42**, 11992–12000.
Guan, J. Q. & Chance, M. R. (2004). In *Encyclopedia of Molecular Cell Biology and Molecular Medicine*, 2nd ed., edited by R. Meyers. New York: Wiley.
Guan, J. Q. & Chance, M. R. (2005). *Trends Biochem. Sci.* **30**, 583–592.
Gupta, S., Mangel, W. F., Sullivan, M., Takamoto, K. & Chance, M. R. (2005). *Synchrotron Rad. New*, **18**, 25–34.
Johnson, K. A. (1986). *Methods Enzymol.* **134**, 677–705.
Johnson, K. A. (1995). *Methods Enzymol.* **249**, 38–61.
Kiselar, J. G., Janmey, P. A., Almo, S. C. & Chance, M. R. (2003*a*). *Mol. Cell Proteom.* **2**, 1120–1132.
Kiselar, J. G., Janmey, P. A., Almo, S. C. & Chance, M. R. (2003*b*). *Proc. Natl. Acad. Sci. USA*, **100**, 3942–3947.
Kiselar, J. G., Maleknia, S. D., Sullivan, M., Downard, K. M. & Chance, M. R. (2002). *Int. J. Radiat. Biol.* **78**, 101–114.
Kiselar, J. G., Mahaffy, R., Pollard, T. D., Almo, S. C. & Chance, M. R. (2007). *Proc Natl. Acad. Sci. USA*, **104**, 1552–1557.
Kwok, L.W., Shcherbakova, I., Lamb, J. S., Park, H. Y., Andresen, K., Smith, H., Brenowitz, M. & Pollack, L. (2006). *J. Mol. Biol.* **355**, 282–293.
Maleknia, S. D., Brenowitz, M. & Chance, M. R. (1999). *Anal. Chem.* **71**, 3965–3973.
Maleknia, S. D., Ralston, C. Y., Brenowitz, M. D., Downard, K. M. & Chance, M. R. (2001). *Anal. Biochem.* **289**, 103–115.
Ralston, C. Y., Sclavi, B., Sullivan, M., Deras, M. L., Woodson, S. A., Chance, M. R. & Brenowitz, M. (2000). *Methods Enzymol.* **317**, 353–368.
Sclavi, B., Sullivan, M., Chance, M. R., Brenowitz, M. & Woodson, S. A. (1998). *Science*, **279**, 1940–1943.
Sclavi, B., Woodson, S., Sullivan, M., Chance, M. & Brenowitz, M. (1998). *Methods Enzymol.* **295**, 379–402.
Sclavi, B., Woodson, S., Sullivan, M., Chance, M. R. & Brenowitz, M. (1997). *J. Mol. Biol.* **266**, 144–159.
Shcherbakova, I., Gupta, S., Chance, M. R. & Brenowitz, M. (2004). *J. Mol. Biol.* **342**, 1431–1442.

Shcherbakova, I., Mitra, S., Beer, R. H. & Brenowitz, M. (2006). *Nucl. Acids Res.* **34**, e48.
Silverman, S. K., Deras, M. L., Woodson, S. A., Scaringe, S. A. & Cech, T. R. (2000). *Biochemistry*, **39**, 12465–12475.
Takamoto, K. & Chance, M. (2004). *Encyclopedia of Molecular Cell Biology and Molecular Medicine*, 2nd ed., edited by R. Meyers, pp. 521–548. New York: Wiley.
Takamoto, K. & Chance, M. R. (2006). *Annu. Rev. Biophys. Biomol. Struct.* **35**, 251–276.
Takamoto, K., Chance, M. R. & Brenowitz, M. (2004). *Nucl. Acids Res.* **32**, e119.
Takamoto, K., Das, R., He, Q., Doniach, S., Brenowitz, M., Herschlag, D. & Chance, M. R. (2004). *J. Mol. Biol.* **343**, 1195–1206.
Uchida, T., Takamoto, K., He, Q., Chance, M. R. & Brenowitz, M. (2003). *J. Mol. Biol.* **328**, 463–478.
Xu, G. & Chance, M. R. (2004). *Anal. Chem.* **76**, 1213–1221.
Xu, G. & Chance, M. R. (2005*a*). *Anal. Chem.* **77**, 4549–4555.
Xu, G. & Chance, M. R. (2005*b*). *Anal. Chem.* **77**, 2437–2449.
Xu, G., Kiselar, J., He, Q. & Chance, M. R. (2005). *Anal. Chem.* **77**, 3029–3037.
Xu, G., Takamoto, K. & Chance, M. R. (2003). *Anal. Chem.* **75**, 6995–7007.